Contents lists available at ScienceDirect

Petroleum Science

journal homepage: www.keaipublishing.com/en/journals/petroleum-science



Original Paper

Sedimentary architecture of a sandy braided river: Insights from a flume experiment



Wen-Jie Feng ^{a, *}, Gao Fei-Xiang ^a, Chang-Min Zhang ^a, Qi-Hao Qian ^b, Tai-Ju Yin ^a, Tao Lei ^c, Hua-Zhan Guo ^d, Jie Chen ^d

- ^a School of Geosciences, Yangtze University, Wuhan, 434100, Hubei, China
- ^b Research Institute of Petroleum Exploration & Development, PetroChina, Beijing, 100083, China
- ^c Exploration and Development Research Institute, North China Petroleum Bureau, SINOPEC, Zhengzhou, 450006, Henan, China
- ^d Exploration and Development Research Institute of Qinghai Oilfield Company, PetroChina, Dunhuang, 736202, Gansu, China

ARTICLE INFO

Article history: Received 6 April 2024 Received in revised form 10 June 2024 Accepted 15 July 2024 Available online 19 July 2024

Edited by Jie Hao

Keywords: Sandy braided river Flume experiment Depositional process Temporary deposition Eventually preserved deposits Sedimentary architecture Element scale and relationship

ABSTRACT

Sandy braided river deposits are widely preserved in ancient stratigraphic records and act as a significant type of hydrocarbon reservoir. Due to the frequent and rapid migration of channels within the riverbed, the sedimentary architecture is highly complex. In this paper, a flume experiment was conducted to reveal the detailed depositional process and establish a fine sedimentary architecture model for sandy braided rivers. The result showed that (1) Three types of braid channels, including the lateral migration channel, the confluence channel, and the deep incised channel, were recognized based on geometry, scale, distribution, and spatial patterns; they are interconnected, forming a complex channel network. (2) Braid channels were characterized by lateral migration, abandonment, filling, and chute cutoff. Lateral migration of channels shaped the braid bars and dominated the formation, growth, and reworking of braid bars. (3) Controlled by the fast and frequent variations of the braid channel network, braid bars were continuously formed, reworked, reshaped, and composited of multiple accretions with different types, orientations, scales, and preservation degrees. Symmetrical and asymmetrical braid bars presented significantly different composition patterns. (4) Dominated by the continuous reworking of braid channels, temporary deposits were limited preserved, braid channel deposits account for 54.3 percent of the eventually preserved braided river deposits, and four types of amalgamate patterns were recognized. Braid bars were cut and limited preserved, only accounting for 45.7 percent of the eventually preserved braided river deposits. (5) During the experiment, only 28 percent of near-surface temporary deposits were eventually preserved in fragmented forms with the final experimental braided river; the shape, spatial patterns, and most of the deposits observed during the depositional process were largely reworked and poorly preserved. (6) The scale of eventually preserved braid bars and braid channels is significantly smaller than the temporary deposits from geomorphic observations. The aspect ratio of the eventually preserved braid bars and the width-to-depth ratio of the eventually preserved braid channel are also significantly different from that of the temporary ones measured from topography data. © 2024 The Authors. Publishing services by Elsevier B.V. on behalf of KeAi Communications Co. Ltd. This is an open access article under the CC BY-NC-ND license (http://creativecommons.org/licenses/by-nc-nd/

4.0/).

1. Introduction

Sandy braided river is a common type of river, widely preserved in stratigraphic records from the Paleozoic to the present, and can form large-scale hydrocarbon reservoirs (Castelltort, 2018; Chen et al., 2021; Huggenberger and Regli, 2006; Larue et al., 2023; Li

* Corresponding author. E-mail address: fwj1017@yangtzeu.edu.cn (W.-J. Feng). et al., 2015b; Li et al., 2019; Lunt et al., 2013; Lynds and Hajek, 2006; Martin and Turner, 1998; Zang et al., 2020; Zhang et al., 2010). The sedimentary architecture of braided rivers dominated the distribution of high and low permeability units and muddy interlayers and determined the fluid flow patterns in subsurface reservoirs (Li et al., 2019; Lunt et al., 2004). Therefore, a deep understanding of the sedimentary architecture and scale of sandy braided rivers is crucial for the efficient development of subsurface oil and gas resources (Kelly, 2006; Zhang et al., 2022).

In the early years of braided river research, observations of modern rivers played a significant role in understanding the hydrodynamics and sedimentary model (Cant and Walker, 1978; McKee et al., 1967; Reinfelds and Nanson, 1993; Rust, 1972; Warburton and Davies, 1994; Williams and Rust, 1969). With the application of satellite imagery and ground-penetrating radar in modern sedimentary investigation, detailed sedimentary architecture models and scale database have been constructed (Ashworth et al., 2011; Best et al., 2003; Colombera et al., 2013; Kociuba et al., 2019, 2019, 2019; Kostic and Aigner, 2007; Lunt et al., 2004; Mumpy et al., 2007; Okazaki et al., 2015; Rice et al., 2009; Sambrook Smith et al., 2005, 2006, 2009, 2010; Skelly et al., 2003; Strick et al., 2019; Wooldridge and Hickin, 2005) and employed in the characterization of subsurface reservoirs (Chen et al., 2021; Huggenberger and Regli, 2006; Li et al., 2019; Zang et al., 2020). Although modern braided rivers provide abundant phenomena and data, there are significant differences in sedimentary characteristics and spatial architecture between modern rivers and subsurface reservoirs. Numerous studies have shown that actively deposited sediments near the surface which been widely discovered are often only partially preserved in sedimentary records (Abdel-Fattah, 2021; Lunt et al., 2013; Paola and Borgman, 1991; Sambrook Smith et al., 2009; Van De Lageweg et al., 2013), inevitably rendering modern braided river depositional characteristics, sedimentary architecture, and scales derived from near-surface observations inadequate for characterizing subsurface reservoirs (Bridge, 1993: Lunt et al., 2004).

Compared to modern braided rivers, outcrops provide sedimentary architecture and quantitative scale information closer to subsurface reservoirs (Abdel-Fattah, 2021; Hossain et al., 2023; Labourdette and Jones, 2007; Li et al., 2015a; Li et al., 2015b; Li et al., 2023c; Long, 2006; Puig et al., 2019; Yao et al., 2018). However, due to its limited exposure conditions, complex formation background conditions, and lack of direct evolutionary process information (Egozi and Ashmore, 2009; Jones et al., 2001; Van De Lageweg et al., 2013), they are inadequate to support the construction of sedimentary architecture models and quantitative scale relationships for braided reservoirs (Li et al., 2023a; Lunt et al., 2004; Sambrook Smith et al., 2009).

Flume experiments and numerical simulations were widely used for investigating the hydrodynamics, sedimentary characteristics, evolutional principles and scale of braided rivers (An et al., 2013; Ashmore et al., 2011; Ashmore, 1982; Baar et al., 2020; Egozi and Ashmore, 2009; Hundey and Ashmore, 2009; Kasprak et al., 2015; Leduc et al., 2019, 2015; Li et al., 2023a; Li et al., 2023b; Lunt et al., 2004; Murray and Paola, 2003; Van De Lageweg et al., 2013; Vesipa et al., 2017; Warburton and Davies, 1994; Zhang et al., 2020). Especially in recent years, the application of laser scanning and close-range SfM techniques were used to collect high-precision digital topography data and enhance the quality and frequency of data for sedimentary characteristics observation (Kasprak et al., 2015; Leduc et al., 2019; Van De Lageweg et al., 2013; Vesipa et al., 2017). Numerical simulations further provide datasets with shorter time intervals, longer simulation times, and more comprehensive coverage of hydrodynamic and sedimentological parameters (Baar et al., 2020; Schuurman et al., 2013, 2018; Schuurman and Kleinhans, 2015; Zhang et al., 2020). Focused on the morphologies and morphodynamics, the geometry and its variations, the scale, and their response to boundary conditions were deeply investigated (Li et al., 2023b; Schuurman and Kleinhans, 2015). However, the sedimentary architecture and scale, controlled by complex braid channel behaviors and subject to limited preservation, still require urgent exploration.

In this paper, a flume experiment was conducted under constant

boundary conditions to understand sedimentary architecture, construct a practical sedimentary architecture model, and obtain the scale of architecture elements for subsurface reservoir characterization. During the experiment, a laser scanner (Faro Focus S70) and a set of time-lapse cameras were utilized to connect the topography and image datasets. A virtual 3D architecture model of the experimental braided river was constructed based on the method proposed by Straub et al. (2012). The sedimentary characteristics, the evolution process of a braided river, and the sedimentary architecture and scale of the preserved experimental braided river deposits were discovered in detail.

2. Experimental setup and methods

2.1. Experimental design

The experiment was conducted in a flume setup for braided river simulation. The setup consisted of a sandy bedform, a sediment supplier, a water supplier, a water storage tank, a 3D laser scanner, and three time-lapse cameras (Fig. 1).

The sandy bedform is 8.2 m long and 1.0 m wide; it was a 0.2 m thick, slightly compressed sand flat covered on a fixed slope. A water storage tank with a constant spill height is set at the end of the sandy bedform to store water and keep the water level constant (Fig. 1). During the experiment, sandy sediments were supplied by a screw feeder set at the upper boundary, water was supplied by a water pump set at the bottom of the water storage tank (Fig. 1). To collect topography and image data, a 3D laser scanner and three time-lapse cameras were set above the sandy bedform (Fig. 1). To enhance the quality of topography data, three sites for laser scanning were set to collect point cloud data from different positions and perspectives (Fig. 1(a)).

2.2. Boundary conditions

The initial slope height of the sandy bedform is 7.8 cm, and the slope is about 0.54° (Fig. 1(a)). The initial elevation distribution is presented in Fig. 2. The materials of the bedform and supplied sediments are poorly sorted sand (D50 is 0.3 mm, Fig. 3) which collected from a natural river. The flow rate of the water supply pump is adjustable. During the experiment, the water supply pipeline remains unchanged. Before each simulation run step, the flow rate was measured and kept at 1000 mL/s. The sediment was supplied by an adjustable screw feeder. Before each run step, the sediment supply rate was measured and set as 2.5 g/s. The average water flow velocity during the experiment was 0.12 m/s, and the maximum water depth was 0.025 m. The Froude number Fr is 0.24, and the bulk Reynolds number Re is 2898.54 (Table 1). The two critical dimensionless variables are kept within a suitable range, ensuring the depositional process is similar to that of natural sandy braided rivers.

2.3. Data collection and processing

During the experiment, topography and image of the simulating braided river were collected by a laser scanner (Faro Focus S70) and three time-lapse cameras (Fig. 1). To avoid the influence of water on laser scanning, the experiment was conducted with a 30-min time interval run step. The whole experiment experienced 93 run steps (Table 1). Laser scanning was performed at the end of each run step. Time-lapse photography was conducted once a second. For each run step, three laser scanning point clouds are collected from three different sites.

The processing of topography data is divided into three steps. First, a fixed reference point cloud fuses the three point clouds of

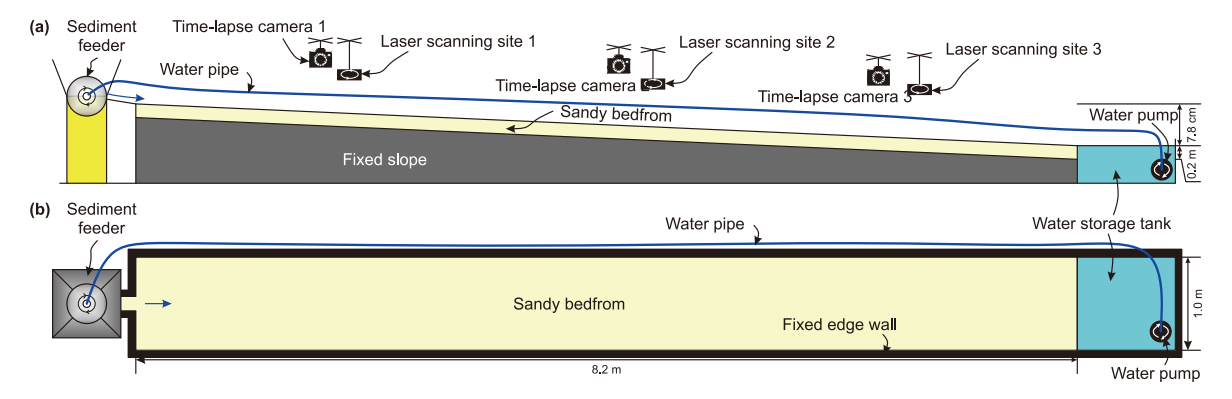


Fig. 1. Schematic diagram of experimental setup ((a) side view of the setup; (b) vertical view of the setup).

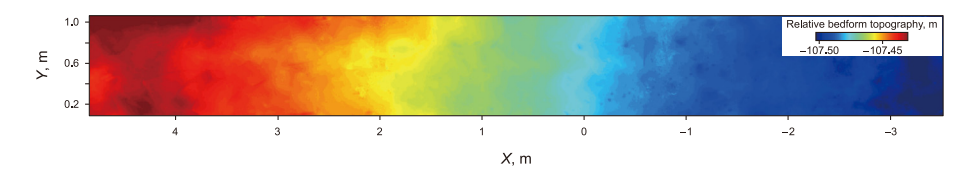


Fig. 2. Initial topography of the sandy bedform (relative height).

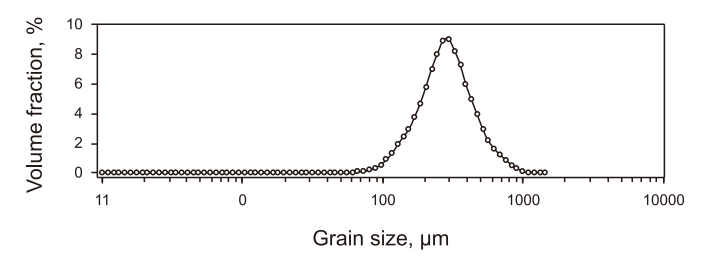


Fig. 3. Grain size distribution of the supplied sediments and bedform materials.

each run step. Then, the points within the range of the simulated braided river are selected for meshing to form a DEM and corresponding orthophoto image. The resolution of the DEM grid is 0.005 m \times 0.005 m. Finally, error correction is performed on the DEM data of 93 run steps based on the topography data within the tank edge wall.

To analyze the morphodynamics and horizontal sedimentary characteristics of the experimental braided river, the detrended topography of each run step was calculated using a fitted downstream element trend. The sediment thickness increment distribution during each run step was analyzed by calculating the topography difference between the current and the previous run step. The sedimentation volume deposited and temporarily preserved in each run step (*V*tp) was calculated.

To discover the sedimentary architecture of the experimental braided river, the final preserved boundary of each run step was

calculated by using the method proposed by Straub et al. (2012) and Van De Lageweg et al. (2013). For each grid cell of the 94 DEMs, the corresponding preserved boundary elevation (*PBE*) was calculated by Eq. (1).

PBE
$$(i, x, y) = \min([DEM (i, x, y), DEM (i+1, x, y), ..., DEM (n, x, y)])$$

 $n = 94, i = 1, ..., n$ (1)

A virtual 3D architecture model of the experimental braided river was constructed based on the PBE data. The 3D model reproduced architectural elements' spatial pattern and geometry that were finally preserved in the experimental braided river. Then, the volume of eventually preserved sediment was calculated during each run step (Vep). Vtp and Vep were used to reveal the linkage between the formation and preservation of sandy deposits. In addition, virtual sedimentary architecture sections located at any position can be extracted from the 3D virtual architecture model. These sections were used for architecture element scale measurement. It is worth noting that the constructed 3D virtual architecture model is likely slightly different from the actual architecture of the experimental braided river (Straub et al., 2012; Van De Lageweg et al., 2013).

3. Results

3.1. Sedimentary characteristics of braiding channels

The experiment fully presented the formation and evolution of a

Table 1Boundary condition of the flume experiment.

| Parameter | Value | Parameter | Value |
|------------------------------|---------|--|-------|
| D50 of supplied sediment, um | 300 | Bedform thickness, m | 0.2 |
| Water discharge, mL/s | 1000 | Slope height, cm | 7.8 |
| Sediment supply rate, g/s | 2.5 | Bedform slope, deg | 0.54 |
| Bedform length, m | 8.2 | Time interval of a run step, min | 30 |
| Bedform width, m | 1.0 | Run steps | 93 |
| Froude number, Fr | 0.24 | The time interval of laser scanning, min | 30 |
| Bulk Reynolds number, Re | 2898.54 | Time interval of time-lapse photography, s | 1 |

typical braided river under constant boundary conditions. The basic sedimentary framework of a sandy braided river can be described as a braid channel network coexisting and interacting with numerous braid bars, evolving in synergy (Figs. 4 and 5).

3.1.1. Complex channel network in a sandy braided river

Based on distribution, geometric shape, and scale, three types of channels were identified from the detrended DEM, including lateral migration channels (LMC), confluence channels (CC), and deep cut channels (DIC) (Figs. 4 and 5). The lateral migration channel developed along the edge of the middle part of the braid bars. The cross-section of the lateral migration channel bedform is usually asymmetric, with one side being deeper and the other side being shallower and continuously migrating laterally under the influence of transverse circulating current. The width of LMC is generally 0.10-0.45 m, the depth is 0.005-0.025 m, and the width-to-depth ratio is about 20/1 (Fig. 5). The confluence channel is formed by the water overflowing onto the braid bars, flowing downstream, and gradually converging (Figs. 4 and 5). Their upstream reaches are shallow and narrow. With the downstream confluence of the upstream reaches, the depth gradually increased. The confluence channel finally merged into the braid channel at the braid bar tail. According to scale measurement based on DEM data, the width of CC is 0.002-0.200 m, the depth is less than 0.002 m, and the widthto-depth ratio is about 15 (Fig. 5). The deep incised channel developed along the edge of the upstream and downstream parts of the braid bar and is significantly deeper than the braid channels (Fig. 5). The width of DIC is 0.1–0.35 m wide, and the depth is 0.01-0.035 m, with a width-to-depth ratio of about 10 (Fig. 5). Along the downstream direction, the lateral migration channels, the confluence channels, and the deep incised channels are connected and form a complex channel network (Figs. 4 and 5).

3.1.2. Channel evolution

During the experiment, the behavior of the complex channel network dominated the river evolution. The sediment thickness increment (Fig. 6) during every run step was calculated using the DEMs to discover the channel activity. Under constant boundary conditions, the channel network changed continuously and rapidly, characterized by lateral migration, abandon, fill, and chute cutoff. Lateral migration of lateral migration channels and deep incised channels dominated the migration and growth of braid bars located

at the two sides of the channel. For every run step, the volume of lateral accretions accounts for over 90% of the total deposition volume (Fig. 6). The width of lateral accretions is roughly equal to the channel width (Fig. 6), which means the channel area nearly kept constant during the experiment. Meanwhile, a small portion of the channel reaches in the channel network was gradually abandoned and filled (Fig. 6). Also, some newly generated channels by chute cutoff caused overflow sedimentation above the existing braid bars (Fig. 6).

3.2. Sedimentary characteristics of braid bars

3.2.1. The formation and evolution of braid bars

The braided channel network undergoes continuous and rapid changes during the simulation process. Controlled by the rapidly changing channel network, braid bars experienced complex formation and evolution processes. Take a reach of the braided river as an example. A continuous observation from run steps 83 to 91 represented a detailed evolution process of a set of braid bars (Fig. 7). There are three main braid bars (Fig. 7(a), braid bars A, B, and C) at the end of run step 83. During the following run step, braid bar A grew by lateral migration of the lateral migration channel C1 (Fig. 7(b)), and B was slightly cut by the lateral migration channel C1 (Fig. 7(b)). Then the larger braid bar A was cut by a newly generated lateral migration channel C2 (Fig. 7(c)), the area of braid bar A decreased and two new braid bars formed (Fig. 7(c), braid bar D and E). At the same time, braid bar B was also cut. During the simulation run step 86, braid bars A and E recomposited, and the lateral migration channel C1 extended (Fig. 7(d)). Affected by the migration of channel C1, braid bars D and F composited. Most of the area of the braid bar F was eroded by C1 (Fig. 7(d)). During the following run step 87, branching of C1 on its upper reach caused the separation of the composited braid bar D+F, and the braid bar F enlarged with the lateral migration of C1 (Fig. 7(e)). Meanwhile, the downstream reach of C1 branching caused the generation of braid bar G and H (Fig. 7(e)). The braid bar F further enlarged during run step 88. During the run step 89 and 90, a new braid bar I formed while the lateral migration channel C1 abandonment and filling (Fig. 7(g)) and then composited with the braid bar F (Fig. 7(h)). During the run step 91, the composited braid bar I + F further enlarged by the lateral migration of a newly generated lateral migration channel C8 (Fig. 7(i)).

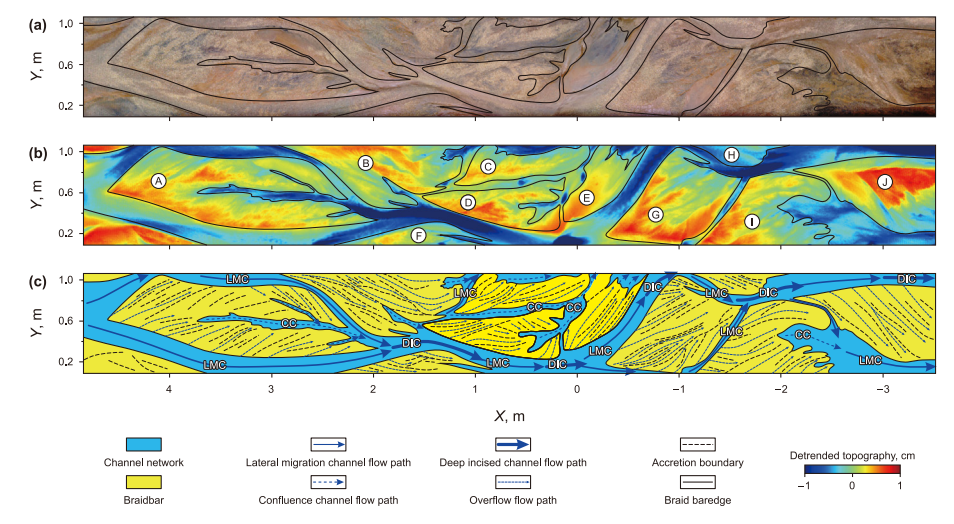


Fig. 4. The orthoimage (a), detrended topography (b), and architecture elements distribution (c) of the experimental braided river at the end of run step 84.

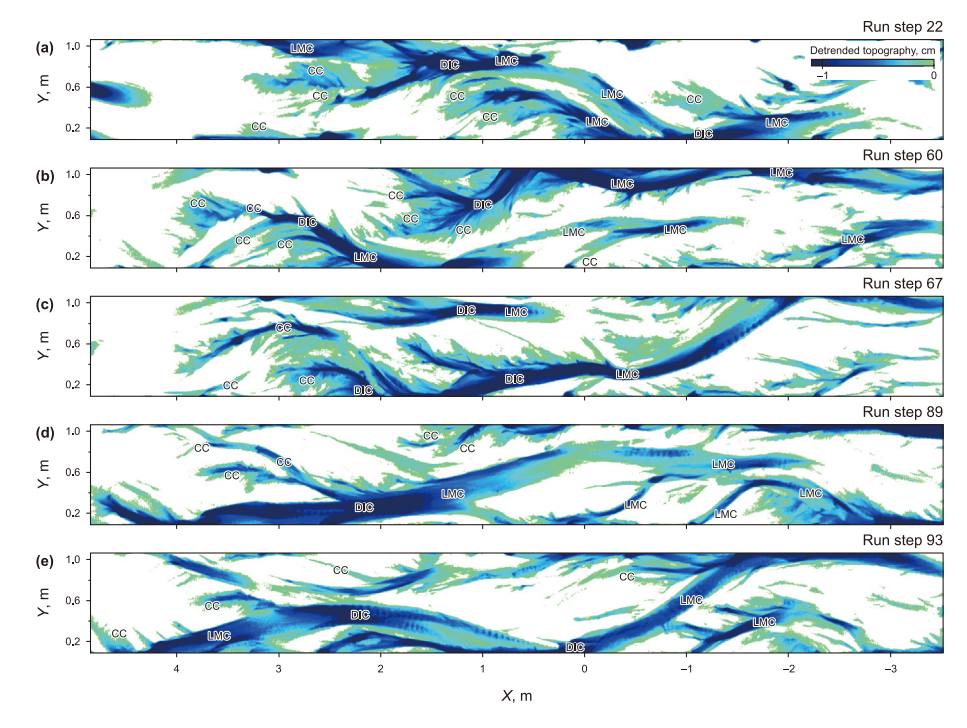


Fig. 5. Characteristics of the complex channel network in the experimental braided river ((a)—(e). The detrended topography at the end of run step 22, 60, 67, 89 and 93, the white area indicates braid bar; BC-braiding channels, DIC-deep incised channel, CC-Confluence channel).

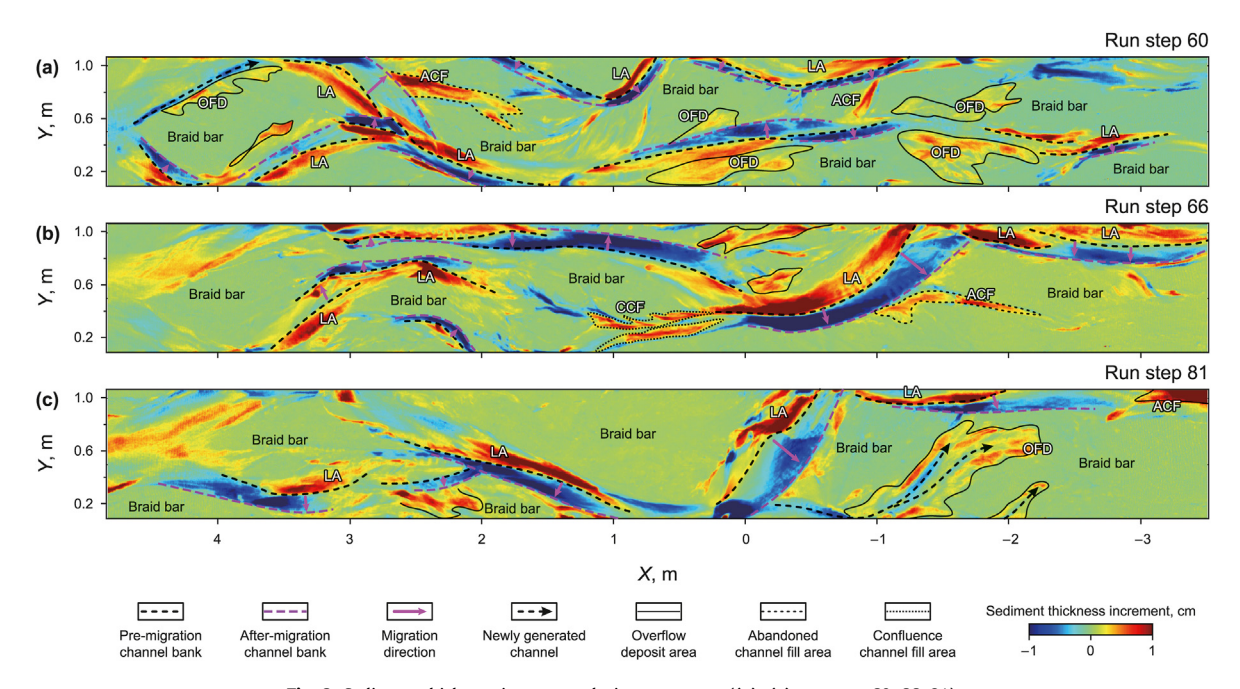


Fig. 6. Sediment thickness increment during a run step ((a)–(c). run step 60, 66, 81).

The experiment presented the continuous and rapid change of the channel network, and braid bars are also subjected to erosion, reworking, and growth. In the channel network, the migration, abandonment, filling, and chute cutoff of different channel reaches usually coexist simultaneously. As a result, the migration, enlargement, erosion, composition, and the new generation of braid bars also coexist during the evolution of a braided river (Fig. 7).

3.2.2. Geomorphological characteristics and internal structures of braid bars

Since the formation and evolution process are continuously affected by different types of channel activity, braid bars can be regarded as a combination of accretion sets with different geometry, patterns, and preservation degrees formed in different run steps. Their internal structure is very complex. Detrended topography reveals the geomorphological characteristics and internal

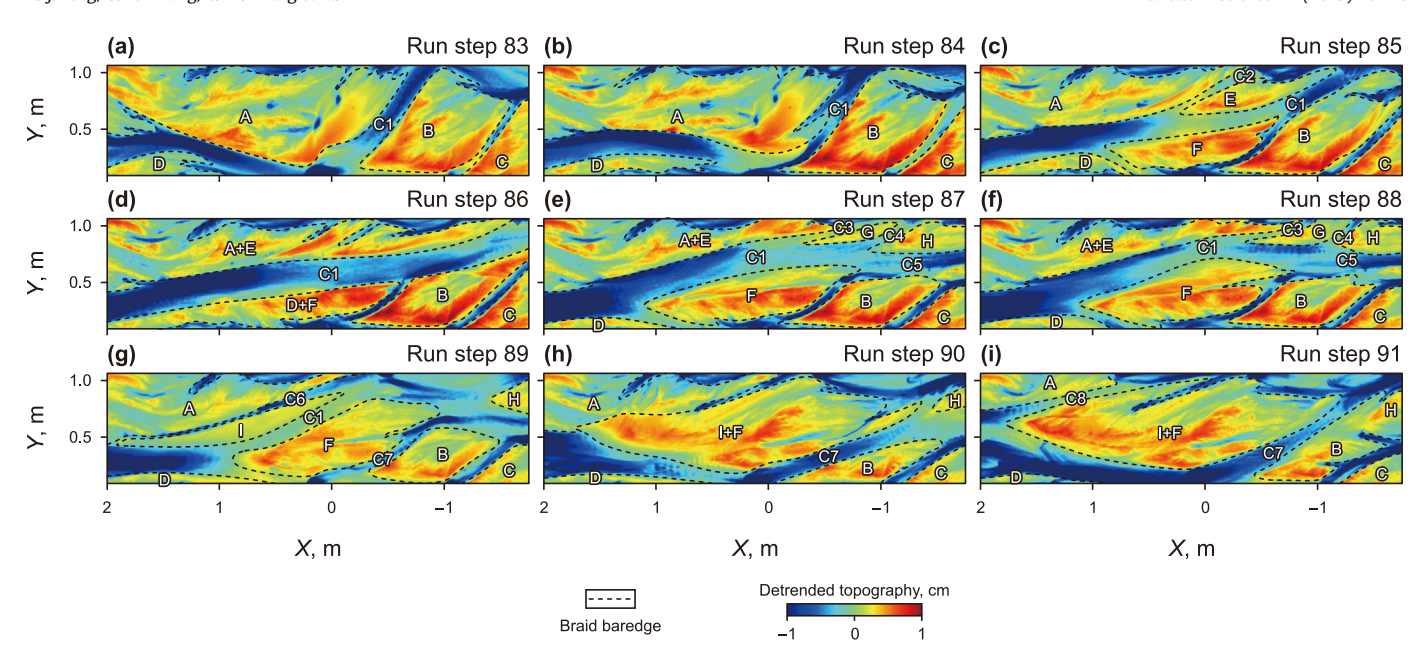


Fig. 7. Formation and evolution of typical braid bars ((a)—(i). The detrended topography of the experimental braided river at the end of run step 83—91, black dashed line is braid bar boundary, the blue area indicated braid channels).

structures of braid bars (Fig. 8). Observations from the detrended topography data suggested that the braid bars combine multiple accretion sets with various migration directions (Fig. 8).

The geometry of the braid bar is divided into symmetric and asymmetric shapes. The symmetric braid bars are composited by multiple accretions with various migration directions and mostly formed at the center of the riverbed (Fig. 8, braid bar A, D, G, H, I, K,

M, N, P, Q). Various migration directions suggest that multiple channels generally control the formation of the symmetric braid bar for a long time. Multiple channels in different run steps intermittently shaped the edge of the symmetric braid bars. In general, two channels simultaneously surround a symmetric braid bar that co-shape the smooth bar boundary. Confluence channels mostly develop in the middle to the downstream of symmetric braid bars.

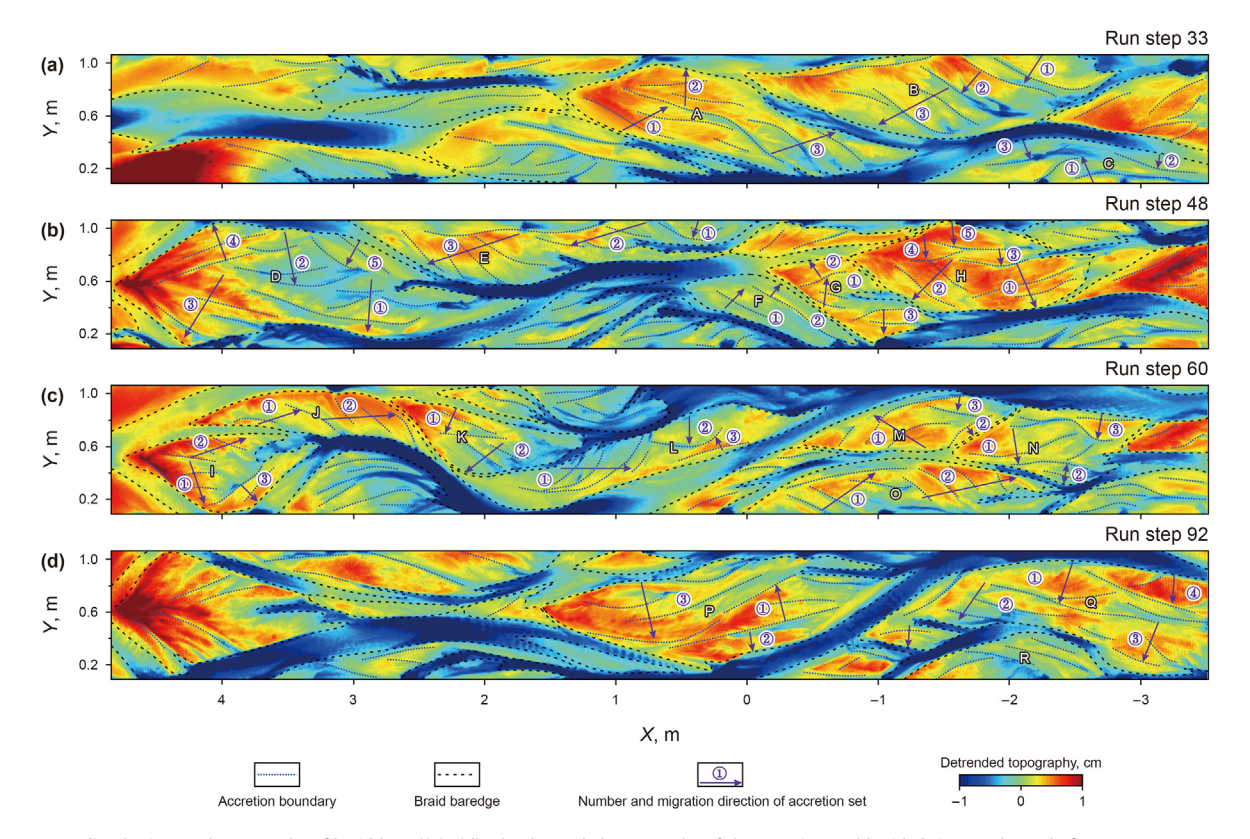


Fig. 8. Geometry, distribution, and topography of braid bars ((a)-(d). The detrended topography of the experimental braided river at the end of run steps 33, 48, 60, and 92).

On the contrary, the asymmetric braid bars are composited by multiple accretions with nearly the same migration and are mostly located near the edge of the riverbed (Fig. 8, braid bar B, C, E, F, J, L, O, R). Asymmetric braid bars are formed by continuous lateral migration of only one lateral migration channel or deep incised channel, and the scale of the associated confluence channel is significantly smaller than that of the symmetric braid bars (Figs. 4 and 8). The migration direction of the asymmetric braid bars is generally upstream (Fig. 8, braid bars B and E) or downstream (Fig. 8, braid bar I) and results in different composition styles. The amalgamation pattern of accretions dominates the heterogeneity and connectivity of the two types of braid bars. Symmetric braid bars have more accretions with various migration directions and more complex amalgamation patterns, resulting in higher heterogeneity and lower connectivity. Although both symmetric and asymmetric braid bars are temporary and will be largely eroded in subsequent sedimentation, the final sedimentary record still partially preserves both types of braid bars. The difference in the number and amalgamation pattern of the accretions of the two types of braid bars will complicate the sedimentary architecture.

3.3. Sedimentary architecture of a braided river

The sedimentary architecture of the experimental braided river was discovered based on the finally preserved boundary elevation during the 93 run steps. Three transversal sections were reconstructed to reveal the sedimentary architecture of the experimental braided river (Fig. 9). Two types of architectural elements (i.e., braid channel and braid bar) were identified by their geometry.

3.3.1. Braid channel

As observation based on detrended topography data, braid channels could be divided into lateral migration channels, deep incised channels, and confluence channels. The channels were identified by the convex bottom geometry on the sedimentary architecture sections (Fig. 9(b2), (c2), (d2)). According to statistics, the lateral migration channels covered 54.3 percent of the three sections. The formation of lateral migration channel deposits undergoes multiple run steps controlled by the active lateral migration channels' lateral migration, vertical cutting, and filling processes. Four types of evolution processes of active lateral migration channels were recognized, including the horizontal lateral migration (Fig. 10 A, D, and G), the upward-lateral migration (Fig. 10 B and C), the vertical cutting and filling (Fig. 10 E, F, and H) and the complex combination of the above three types (Fig. 10 I, J, and K).

The horizontal lateral migration of active channels generated broad amalgamated channelized deposits with significant transversal depth variances (Fig. 10 A, D, and G). The migration is generally unidirectional, indicating the continuous and fast wandering of the lateral migration channels. The upward-lateral migration of braid channels occurred during the gradual abandoning and filling process of a lateral migration or deep incised channel. As a result, the accretion scale gradually decreased (Fig. 10 B and C). A slightly unidirectional lateral migration of the channels was observed (Fig. 10 C).

During the gradual abandoning process, a deep incised channel or a confluence channel was vertically cut and filled. Slightly bidirectional migration of the channels caused frequent deposit cutting and filling (Fig. 10 E, F, and H).

The complex combination of channels occurred during the long-term evolution of one or more channels and formed middle to larger scale channelized deposits (Fig. 10 I, J, and K). Due to the frequent and long-term evolution of channels, the sedimentary architecture of the channel deposition is very complex (Fig. 10).

3.3.2. Braid bar

Braid bars are characterized by flat top and bottom boundaries (Fig. 9). Most of the braid bars were cut by braid channels, consequently, the preservation of braid bars in the final deposits is low in general (Fig. 9). According to the observation of the sections, the braid bars deposited at the early to middle stage of the experiment were poorly preserved, only the late deposited bars were well-preserved (Fig. 9(b1)—(d2)). In addition, no distinctive form exists in the section of the finally preserved experimental braided river. According to statistics, braid bars covered 45.7 percent of the preserved deposits.

4. Discussion

4.1. The temporary deposition and eventual preservation

According to the observations on modern and experimental braided rivers, rapidly and frequently shifting braid channels cut the pre-existing deposits and cause new deposition on the riverbed. The near-surface deposits can be regarded as temporary depositions and would be partially to totally eroded by the later braid channels. As a result, the eventual preservation of deposits formed during a time interval is limited (Ashmore, 1982; Bridge, 1993; Paola and Borgman, 1991; Schumm and Khan, 1972). Quantitative observations on a 3 km reach of the South Saskatchewan River demonstrated the effect of braid channel shifting (Lane et al., 2010). Flume experiments revealed that between 10% and 40% of the mean channel depth was finally preserved (Van De Lageweg et al., 2013).

4.1.1. Limited preservation of temporary depositions

In this paper, the experimental braided river was formed under constant boundary conditions and experienced an autogenic evolution process. The average topography of the experimental braided river continuously increased with the run step (Fig. 11), indicating a steady aggradation of the experimental river. The average sediment thickness of the experimental river is 3 cm (Fig. 11). According to the measurement of braid channel based on topography data, their depth is generally smaller than 1.5 cm (Fig. 10). Under constant boundary conditions, the depth of braid channels kept stable. Therefore, braid channel incision played an important role in the preservation of pre-existing deposits. Transversal sections revealed that the braid channels incised into the deposits, which formed during several to tens of run steps before (Fig. 9).

Take the deposits formed during run step 66 as an example (Fig. 12). Temporary deposits were distributed along the braid channels and covered about 19.73 percent of the riverbed area (Fig. 12(a)). After the experiment, eventually preserved deposits that formed during run step 66 only covered 5.65 percent of the riverbed area. Similar phenomena were observed throughout the simulation process (Fig. 13), resulting in temporary deposits formed during each run step being preserved to a limited proportion and in fragmented forms within the experimental braided river deposits. Numerous flume experiments also observed the low preservation of temporary depositions (Ashmore, 1982; Bridge, 1993; Schumm and Khan, 1972; Van De Lageweg et al., 2013). The eventually preserved depositional bodies were characterized by fragmented shapes, discontinuous distributions, various contact relationships, and complicated architectural patterns (Fig. 14). That means the majority of the braid bars were reworked by later channels, braid bars observed during the experiment were not well preserved (Fig. 9). Outcrop observations also revealed the poor preservation of braid bars (Jones et al., 2001; Kelly, 2006).

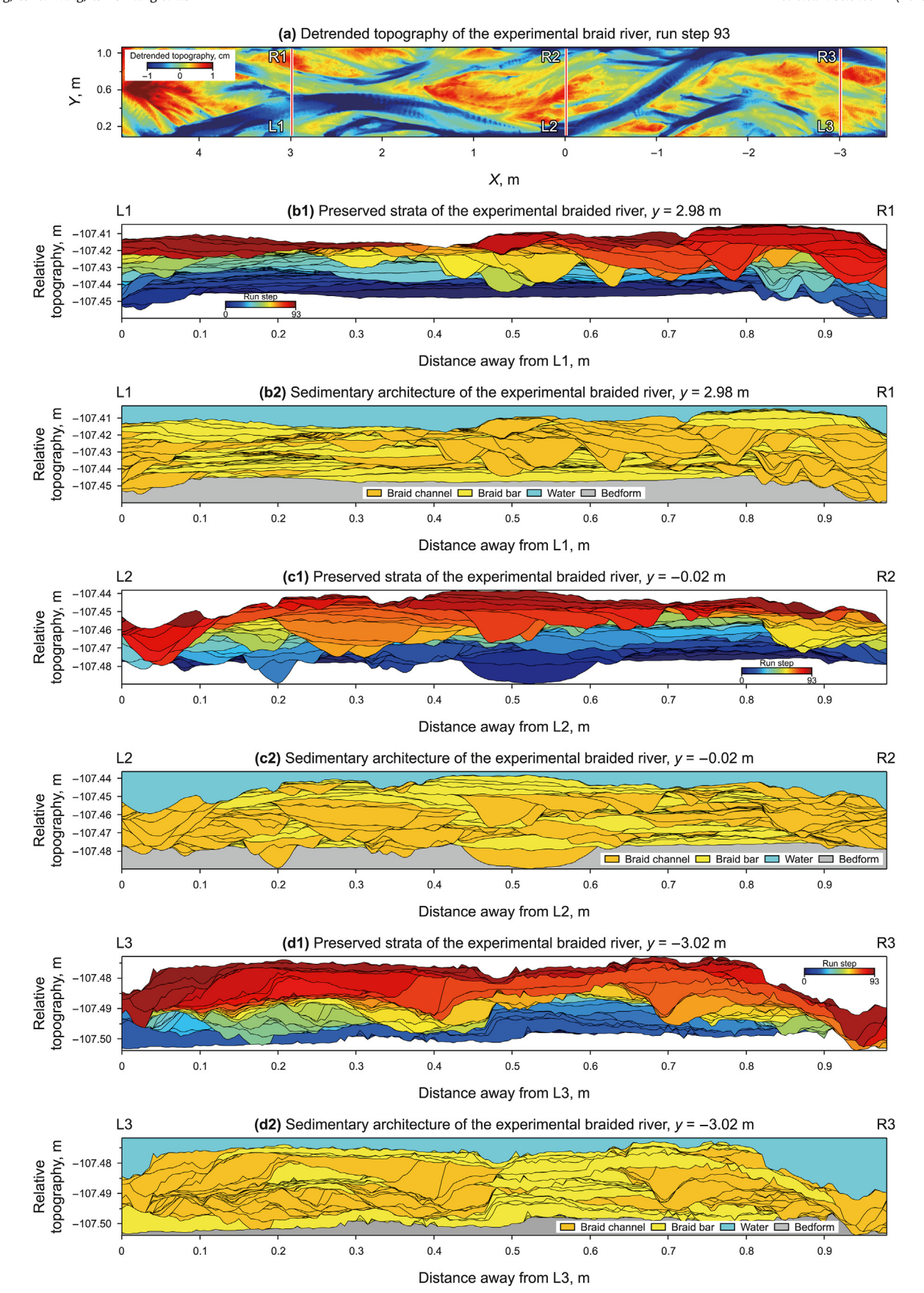


Fig. 9. Sedimentary architecture of the experimental braided river (a). detrended topography; (b1) Preserved strata of section L1–R1; (b2) Sedimentary architecture of section L1–R1; (c1) Preserved strata of section L3–R3; (d2) Sedimentary architecture of section L3–R3; (d2) Sedimentary architecture of section L3–R3; (d3) Sedimentary architecture of section L3–R3;

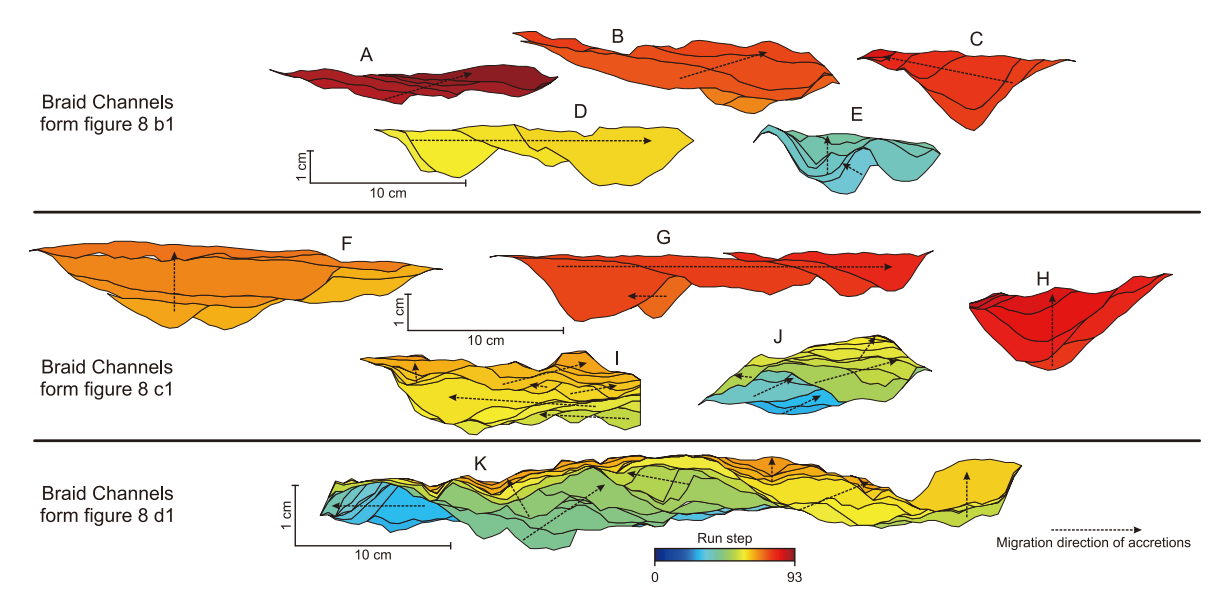


Fig. 10. Spatial patterns of typical braid channels.

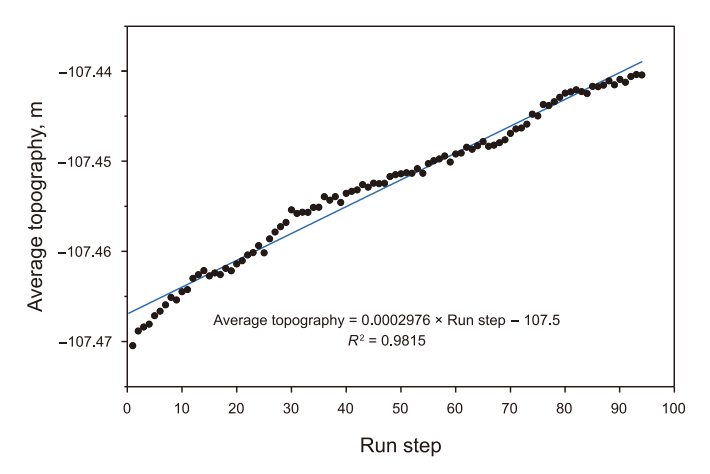


Fig. 11. Average topography of the experimental braided river.

4.1.2. Variations of preservation during the experimental braided river evolution

To quantitatively analyze the difference between the temporary deposition and eventual preservation during the evolution of the experimental braided river, the volume of temporary and eventually preserved deposits (*V*tp and *V*ep) in each run step was calculated (Fig. 15). During the experiment, *V*tp fluctuates around

0.0088 m³ and indicates that the deposition of the experimental braided river was sustained and generally stable. Unlike the stability of *V*tp, *V*ep remains stable until the end of run step 78 and gradually increases to be equal to *V*tp in subsequent run steps (Fig. 15).

The ratio of Vep to Vtp was also calculated, the result suggested that only 33.45 percent of the temporary deposits were eventually preserved in the experimental braided river. We noticed that the Vep/Vtp experienced three stages during the experiment (Fig. 15). The first stage lasted from run steps 1 to 7, and Vep/Vtp decreased from 0.60 to 0.28. The following stage lasts from run step 8 to 78, and the Vep/Vtp fluctuates around 0.28. That means only 28 percent of the temporary deposits were eventually preserved on average. The later stage lasts from run step 79 to 93 and is characterized by an increasing Vep/Vtp from 0.28 to 1.00. It is revealed that shifting and incising of braid channels may cut a large content of the pre-existing deposits. The temporary deposits were repeatedly cut by subsequent channel activities and ultimately partially preserved due to riverbed aggradation. The closer the time the temporary deposits formed, the lower the proportion would be cut (Fig. 15). Variations of Vep/Vtp revealed the vertical preservation difference. Channels slightly reworked the upper part of braided river deposits compared to the middle to the bottom part. The riverbed aggradation rate and braid channel depth dominated the eventual preservation rate of deposits.

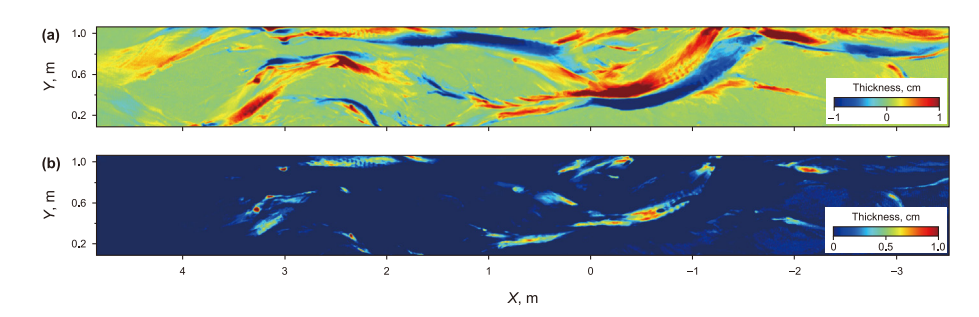


Fig. 12. Distribution of temporary deposited and eventually preserved depositions in run step 66. (a) Sediment thickness increment (run step 66), (b) The thickness of finally preserved deposits (run step 66).

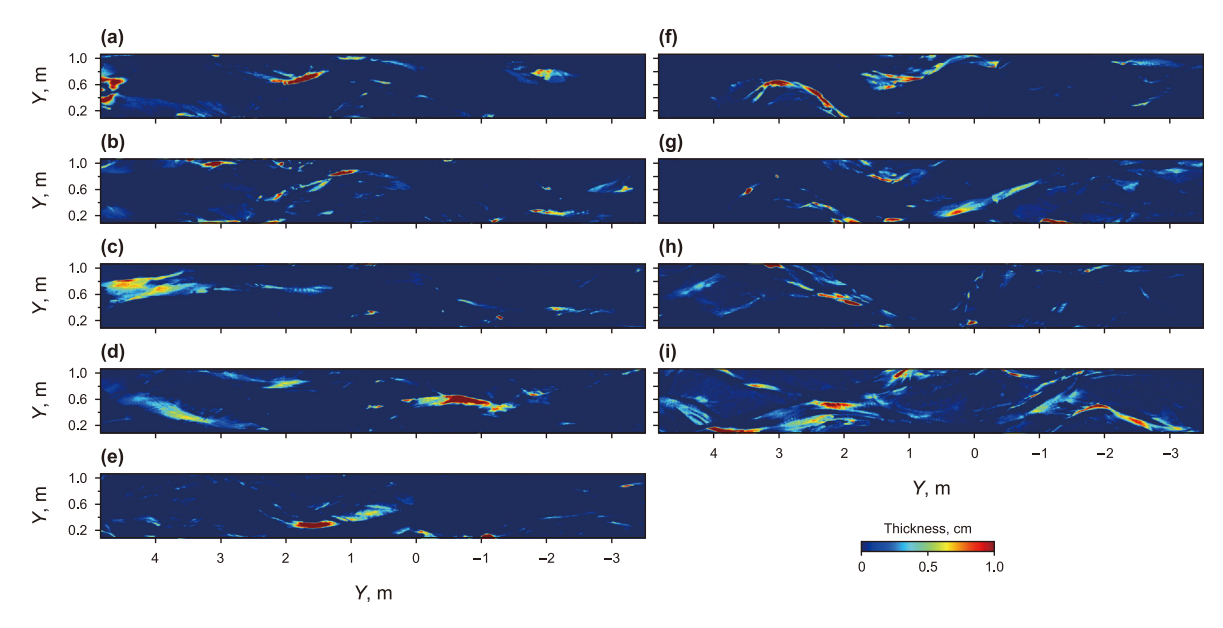


Fig. 13. Distribution of deposits formed within a run step and eventually preserved in the experimental braided river. (a)—(i) run steps 12, 22, 32, 42, 52, 62, 72, 82 and 92.

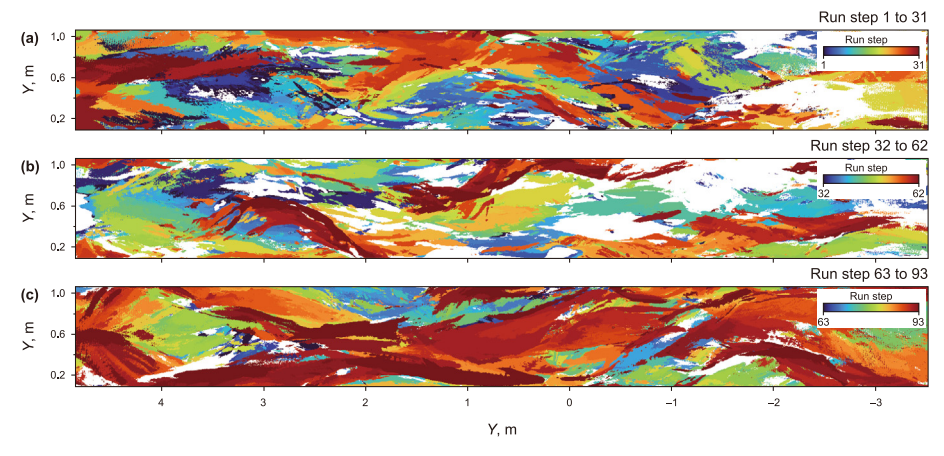


Fig. 14. Distribution of eventually preserved deposits formed in running steps 1 to 93. (a) run steps 1 to 31, (b) run steps 32 to 62, (c) run steps 63 to 93. The preserved deposits were colored by corresponding run steps.

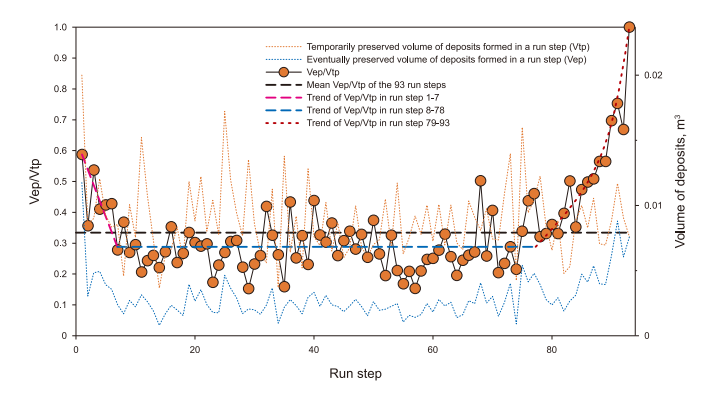


Fig. 15. The trend of volume temporary and eventually preserved deposits.

4.2. Scale of architecture elements

To accurately characterize the architecture of subsurface braided river reservoir, the scale and relationships of braid bars and

channels and their internal bed sets and stories were discovered in numerous studies (Best et al., 2003; Kelly, 2006; Li et al., 2023a; Li et al., 2023b; Sambrook Smith et al., 2009, 2005; Zang et al., 2020). The scale invariant characteristics observed in fluvial systems and their deposits suggest that empirical predictions of key variables such as braid bar width and length can be made if additional data are known or can be reasonably estimated (Kelly, 2006). According to the comparison of bed sets and stories scale of young and old deposits of a modern braided river, older deposits' scale and quantitative relationship are closer to that of the ancient sedimentary records (Sambrook Smith et al., 2009). In this paper, the experiment also revealed that the sedimentary architecture of the eventually preserved older deposits is more similar to that of the ancient sedimentary records (Fig. 9).

4.2.1. Braid bar scale

We measured the braid bars in modern braided rivers and the temporary braid bars in the experimental braided rivers, and the result demonstrated that the relationship between braid bar length and width is highly consistent (Fig. 16). Scale invariance of braid

bars indicated the reliability of the experimental braided river. However, the eventually preserved braid bar scale measured based on the reconstructed sedimentary architecture sections (partially shown in Fig. 9) revealed that the length and width of the eventually preserved braid bar is largely smaller than that of the temporary braid bars, the relationship of length and width is also significantly varied (Fig. 16).

4.2.2. Braid channel scale

The braid channel scale was also measured based on detrend topography and reconstructed sedimentary architecture sections. Results suggested that there are significant differences in width, depth, and aspect ratio among the lateral migration channel, the deep-incised channel, and confluence channel (Fig. 17). The lateral migration channels were the widest, followed by the deep-incised channel and the narrowest is the confluence (Fig. 17). The deeply incised channel was significantly deeper than that of the lateral migration and confluence channels (Fig. 17). However, the eventually preserved channels (measured from transversal sections, SMC) is significantly narrow than the above three types of channels. The depth of the eventually preserved channels was close to the lateral migration channels and smaller than that of the deeply incised channels (Fig. 17). That is because the temporary channels measured based on topography data were reworked or eroded by later channels. In summary, the scale of eventually preserved braid channels and braid bars is significantly smaller than that of the temporary channels and bars.

4.3. Limitations

Although research on modern braided rivers, numerical and physical simulated braided rivers has explored the sedimentary characteristics of braid bars (Bridge, 1993; Bristow and Best, 1993; Li et al., 2023b; Mumpy et al., 2007; Sambrook Smith et al., 2006; Skelly et al., 2003), established detailed sedimentary architecture models (Best et al., 2003; Bridge and Lunt, 2006; Lunt et al., 2004; Sambrook Smith et al., 2009; Zang et al., 2020), and further obtained a large amount of scale data and aspect ratio (Kelly, 2006; Li et al., 2023b), these understandings may not be able to be used to understand braided river sedimentation in stratigraphic records, nor can they effectively assist in characterizing subsurface oil and

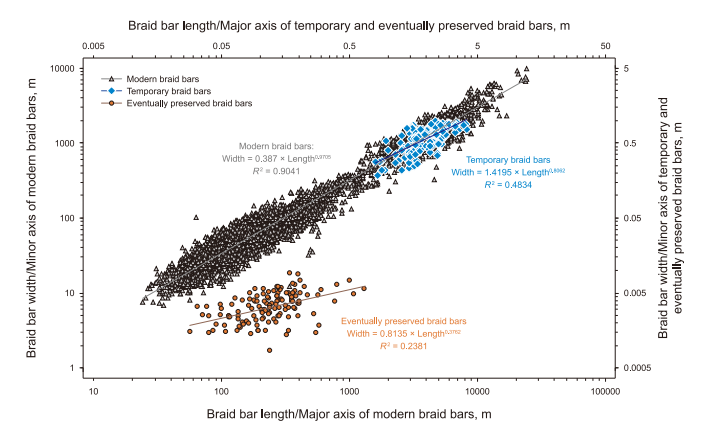


Fig. 16. Comparison of modern and experimental braid bars. Modern braid bar scale data was measured based on satellite images of the Markham River in eastern Papua New Guinea, the South Saskatchewan River and the Platte River in Canada, the Lena River in Russia, the Rakaia River and the Waimakariri River in New Zealand, the Brahmaputra River and the Tista River in India. Experimental braid bars were divided into two types: the temporary braid bars were measured based on detrended topography, and the eventually preserved braid bars were measured based on the transversal sedimentary architecture sections.

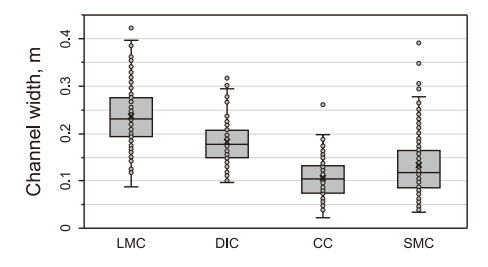
gas reservoirs.

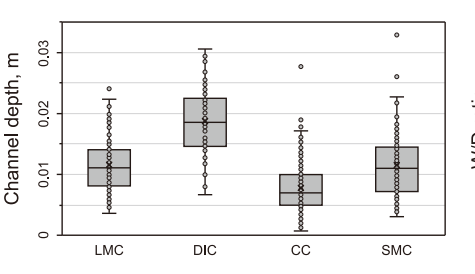
Investigation of experimental data and outcrop was necessary to construct a practical and quantitative sedimentary architecture model. In this paper, the experiment reveals the significant difference between temporary deposits and eventual preservation. However, the main controlling factors and mechanisms of this difference still need to be explored. To build a reliable sedimentary architecture model and a predictable scale relationship, more experiments and outcrop data are urgently needed.

5. Conclusion

This paper describes a flume experiment conducted to investigate the sedimentary characteristics and architecture of a sandy braided river. Observations on modern and experimental braided rivers show that although the morphological patterns remain stable, the rapid and frequent migration of braid channels and bars has led to the complexity of sedimentary architecture. The investigation based on the experimental braided river suggests that.

- (1) Based on the distribution, flow pattern, and geometry, three types of braid channels were recognized: the lateral migration channels, the confluence channels, and the deep incised channels. Interconnected channels formed a complex network with significant water depth, channel width, and spatial pattern variances.
- (2) The channel network changed continuously and rapidly and was characterized by lateral migration, abandonment, filling, and chute cutoff. Lateral migration of channels dominated the evolution of braid bars. Abandoned channel filling and chute cutoff only occurred in limited river reach.
- (3) During the experiment, the formation and evolution of braid bars experienced repetitious formation, composition, and reworking. Braid bars were composed of multiple accretions. Two types of braid bars were recognized from the experimental braided river. The symmetric braid bars are composited by multiple accretions with various migration directions and are mostly formed at the center of the riverbed. The asymmetric braid bars are composited by multiple accretions with nearly the same migration and are mostly located near the edge of the riverbed.
- (4) A 3D virtual architecture model reconstructed based on PBE data revealed that the proportion of braid channel sedimentation can reach 54.3% of the eventually preserved braided river deposits. There are four channel sedimentation types: horizontal lateral migration, upward-lateral migration, vertical cutting and filling, and the complex combination of the above three types. The amalgamation of braid channel sedimentation makes the eventually preserved channel deposits times wider than the channels observed through morphology measurement. Braid bars were cut by channels in general and limited preserved, and the braid bars account for 45.7% of the experimental braided river.
- (5) Due to the fast and frequent migration of braid channels, most of the near-surface deposits were reworked, and only 28% of the temporary deposits were eventually preserved in fragmented forms within the experimental braided river.
- (6) The scale of braid bars measured from experimental topography data indicated the scale invariance of braided river deposits. The scale of the eventually preserved braid bars is significantly smaller than the temporary braid bars. The aspect ratio of temporary and eventually preserved braid bars is different. The scale of eventually preserved braid channels also significantly differs from the channels measured from topography data.





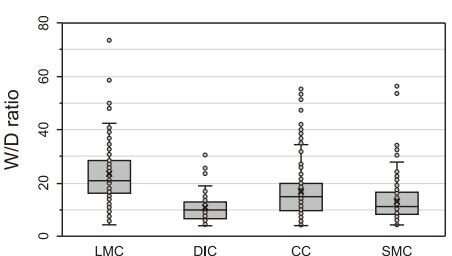


Fig. 17. Width, depth, and width/depth ratio of the lateral migration channel (LMC), the deep incised channel (DIC), the confluence channel (CC), and the channel measured from transversal sections (SMC) of the experimental braided river.

(7) This experiment reveals the significant difference in sedimentary architecture, scale and quantitative relationship between temporary deposits and eventually preserved sedimentary records. Results suggested that the geometry, spatial patterns, scale, and corresponding quantitative relationship of architectural elements observed from modern braided rivers cannot be used for subsurface reservoir prediction. A predictable quantitative architecture model should be exacted from outcrop and experimental data instead of modern river morphology in subsurface reservoir characterization.

CRediT authorship contribution statement

Wen-Jie Feng: Writing — review & editing, Writing — original draft, Visualization, Software, Project administration, Methodology, Investigation, Formal analysis, Data curation. Gao Fei-Xiang: Writing — original draft, Visualization, Software, Methodology, Data curation. Chang-Min Zhang: Writing — review & editing, Supervision, Funding acquisition, Data curation. Qi-Hao Qian: Software, Methodology, Data curation. Tai-Ju Yin: Supervision, Software, Methodology. Tao Lei: Writing — review & editing, Validation, Software, Resources. Hua-Zhan Guo: Writing — review & editing, Visualization, Validation, Data curation. Jie Chen: Writing — review & editing, Visualization, Software, Investigation.

Declaration of generative AI and AI-assisted technologies in the writing process

During the preparation of this work the authors used Grammarly in order to improve the language. After using this tool/service, the authors reviewed and edited the content as needed and take full responsibility for the content of the publication.

Declaration of competing interest

The authors declare that they have no known competing financial interests or personal relationships that could have appeared to influence the work reported in this paper.

Acknowledgement

This study is funded by two projects of the National Natural Science Foundation of China (No. 41802123, 42130813).

References

Abdel-Fattah, Z.A., 2021. Fluvial architecture of the Upper Cretaceous Nubia Sandstones: an ancient example of sandy braided rivers in central Eastern Desert, Egypt. Sediment. Geol. 420, 105923. https://doi.org/10.1016/ i.sedgeo.2021.105923.

An, H.P., Chen, S.C., Chan, H.C., et al., 2013. Dimension and frequency of bar

formation in a braided river. Int. J. Sediment Res. 28, 358–367. https://doi.org/10.1016/S1001-6279(13)60046-3.

Ashmore, P., Bertoldi, W., Tobias Gardner, J., 2011. Active width of gravel-bed braided rivers. Earth Surf. Process. Landforms 36, 1510–1521. https://doi.org/10.1002/esp.2182

Ashmore, P.E., 1982. Laboratory modelling of gravel braided stream morphology. Earth Surf. Process, Landforms 7, 201–225. https://doi.org/10.1002/esp.3290070301.

Ashworth, P.J., Sambrook Smith, G.H., Best, J.L., et al., 2011. Evolution and sedimentology of a channel fill in the sandy braided South Saskatchewan River and its comparison to the deposits of an adjacent compound bar. Sedimentology 58, 1860–1883. https://doi.org/10.1111/j.1365-3091.2011.01242.x.

Baar, A.W., Weisscher, S.A.H., Kleinhans, M.G., 2020. Interaction between lateral sorting in river bends and vertical sorting in dunes. Sedimentology 67, 606–626. https://doi.org/10.1111/sed.12656.

Best, J.L., Ashworth, P.J., Bristow, C.S., et al., 2003. Three-dimensional sedimentary architecture of a large, mid-channel sand braid bar, Jamuna River, Bangladesh. J. Sediment. Res. 73, 516–530. https://doi.org/10.1306/010603730516.

Bridge, J.S., 1993. The interaction between channel geometry, water flow, sediment transport and deposition in braided rivers. Geological Society. London, Special Publications 75, 13–71. https://doi.org/10.1144/GSL.SP.1993.075.01.02.

Bridge, J.S., Lunt, I.A., 2006. Depositional models of braided rivers. In: Sambrook Smith, G.H., Best, J.L., Bristow, C.S., Petts, G.E. (Eds.), Braided Rivers. Wiley, Hoboken, pp. 11–50. https://doi.org/10.1002/9781444304374.ch2.

Bristow, C.S., Best, J.L., 1993. Braided rivers: perspectives and problems. Geological Society. London, Special Publications 75, 1–11. https://doi.org/10.1144/

Cant, D.J., Walker, R.G., 1978. Fluvial processes and facies sequences in the sandy braided South Saskatchewan River, Canada. Sedimentology 25, 625–648. https://doi.org/10.1111/j.1365-3091.1978.tb00323.x.

Castelltort, S., 2018. Empirical relationship between river slope and the elongation of bars in braided rivers: a potential tool for paleoslope analysis from subsurface data. Mar. Petrol. Geol. 96, 544–550. https://doi.org/10.1016/j.marpetgeo.2018.05.008.

Chen, X., Xu, S.Y., Li, S.M., et al., 2021. Identification of architectural elements based on SVM with PCA: a case study of sandy braided river reservoir in the Lamadian Oilfield, Songliao Basin, NE China. J. Petrol. Sci. Eng. 198, 108247. https://doi.org/ 10.1016/j.petrol.2020.108247.

Colombera, L., Mountney, N.P., McCaffrey, W.D., 2013. A quantitative approach to fluvial facies models: methods and example results. Sedimentology 60, 1526–1558. https://doi.org/10.1111/sed.12050.

Egozi, R., Ashmore, P., 2009. Experimental analysis of braided channel pattern response to increased discharge. J. Geophys. Res. 114, 2008JF001099. https:// doi.org/10.1029/2008JF001099.

Hossain, S., Shekhar, H., Rahman, N., 2023. Facies and architectural element analysis of the upper bokabil sandstone in the bengal basin. Sediment. Geol. 453, 106433. https://doi.org/10.1016/j.sedgeo.2023.106433.

Huggenberger, P., Regli, C., 2006. A sedimentological model to characterize braided river deposits for hydrogeological applications. In: Sambrook Smith, G.H., Best, J.L., Bristow, C.S., Petts, G.E. (Eds.), Braided Rivers. Wiley, Hoboken, pp. 51–74. https://doi.org/10.1002/9781444304374.ch3.

Hundey, E.J., Ashmore, P.E., 2009. Length scale of braided river morphology. Water Resour. Res. 45, 2008WR007521. https://doi.org/10.1029/2008WR007521.

Jones, S.J., Frostick, L.E., Astin, T.R., 2001. Braided stream and flood plain architecture: the rio vero formation, Spanish pyrenees. Sediment. Geol. 139, 229–260. https://doi.org/10.1016/S0037-0738(00)00165-2.

Kasprak, A., Wheaton, J.M., Ashmore, P.E., et al., 2015. The relationship between particle travel distance and channel morphology: results from physical models of braided rivers. J. Geophys. Res. Earth Surface 120, 55–74. https://doi.org/ 10.1002/2014IF003310.

Kelly, S., 2006. Scaling and hierarchy in braided rivers and their deposits: examples and implications for reservoir modelling. In: Sambrook Smith, G.H., Best, J.L., Bristow, C.S., Petts, G.E. (Eds.), Braided Rivers. Wiley, Hoboken, pp. 75–106. https://doi.org/10.1002/9781444304374.ch4.

Kociuba, W., Janicki, G., Dyer, J.L., 2019. Contemporary changes of the channel pattern and braided gravel-bed floodplain under rapid small valley glacier recession (Scott River catchment, Spitsbergen). Geomorphology 328, 79–92. https://doi.org/10.1016/j.geomorph.2018.12.008.

- Kostic, B., Aigner, T., 2007. Sedimentary architecture and 3D ground-penetrating radar analysis of gravelly meandering river deposits (Neckar Valley, SW Germany). Sedimentology 54, 789–808. https://doi.org/10.1111/j.1365-3091.2007.00860.x.
- Labourdette, R., Jones, R.R., 2007. Characterization of fluvial architectural elements using a three-dimensional outcrop data set: escanilla braided system, South-Central Pyrenees, Spain. Geosphere 3, 422. https://doi.org/10.1130/GES00087.1.
- Lane, S.N., Widdison, P.E., Thomas, R.E., et al., 2010. Quantification of braided river channel change using archival digital image analysis. Earth Surf. Process. Landforms 35, 971–985. https://doi.org/10.1002/esp.2015.
- Larue, D.K., Allen, J., Beeson, D., et al., 2023. Fluvial reservoir architecture, directional heterogeneity and continuity, recognizing incised valley fills, and the case for nodal avulsion on a distributive fluvial system: kern River field, California. Bulletin 107, 477–513. https://doi.org/10.1306/09232220163.
- Leduc, P., Ashmore, P., Gardner, J.T., 2015. Grain sorting in the morphological active layer of a braided river physical model. Earth Surface Dynamis 3, 577–585. https://doi.org/10.5194/esurf-3-577-2015.
- Leduc, P., Peirce, S., Ashmore, P., 2019. Short communication: challenges and applications of structure-from-motion photogrammetry in a physical model of a braided river. Earth Surface Dynamis 7, 97–106. https://doi.org/10.5194/esurf-7-97-2019.
- Li, H.Y., Gao, Y., Wang, Y.J., et al., 2015a. Intercalation pattern and its impact on development of braided river reservoirs: a case of Fengcheng Oilfield, Junggar Basin, NW China. Petrol. Explor. Dev. 42, 397–407. https://doi.org/10.1016/ S1876-3804(15)30031-8.
- Li, H.C., Li, J.H., Li, Z.D., 2023a. Quantitative scale analysis of the channel bar in a braided river and its internal architecture. Appl. Sci. 14, 257. https://doi.org/ 10.3390/app14010257.
- Li, S.L., Yu, X.H., Chen, B.T., Li, et al., 2015b. Quantitative characterization of architecture elements and their response to base-level change in a sandy braided fluvial system at a mountain front. J. Sediment. Res. 85, 1258–1274. https://doi.org/10.2110/isr.2015.82.
- Li, W., Colombera, L., Yue, D.L., et al., 2023b. Controls on the morphology of braided rivers and braid bars: an empirical characterization of numerical models. Sedimentology 70, 259–279. https://doi.org/10.1111/sed.13040.
- Li, W., Yue, D.L., Du, Y.S., et al., 2023c. Controls of accommodation to sedimentsupply ratio on sedimentary architecture of continental fluvial successions. Petrol. Sci. 20 (4), 1961–1977. https://doi.org/10.1016/j.petsci.2023.02.015.
- Li, Z.D., Pang, H., Xu, J.Z., et al., 2019. Case study of sandbody architecture and quantitative parameters of the far-source sandy braided river: saertu Oilfield, Daqing, China. J. Petrol. Sci. Eng. 181, 106249. https://doi.org/10.1016/ j.petrol.2019.106249.
- Long, D.G.F., 2006. Architecture of pre-vegetation sandy-braided perennial and ephemeral river deposits in the Paleoproterozoic Athabasca Group, northern Saskatchewan, Canada as indicators of Precambrian fluvial style. Sediment. Geol. 190, 71–95. https://doi.org/10.1016/j.sedgeo.2006.05.006.
- Lunt, I.A., Bridge, J.S., Tye, R.S., 2004. A quantitative, three-dimensional depositional model of gravelly braided rivers. Sedimentology 51, 377–414. https://doi.org/ 10.1111/j.1365-3091.2004.00627.x.
- Lunt, I.A., Sambrook Smith, G.H., Best, J.L., et al., 2013. Deposits of the sandy braided South Saskatchewan River: implications for the use of modern analogs in reconstructing channel dimensions in reservoir characterization. Bulletin 97, 553–576. https://doi.org/10.1306/09251211152.
- Lynds, R., Hajek, E., 2006. Conceptual model for predicting mudstone dimensions in sandy braided-river reservoirs. Bulletin 90, 1273—1288. https://doi.org/10.1306/03080605051.
- Martin, C.A.L., Turner, B.R., 1998. Origins of massive-type sandstones in braided river systems. Earth Sci. Rev. 44, 15–38. https://doi.org/10.1016/S0012-8252(98) 00019-1.
- McKee, E.D., Crosby, E.J., Berryhill, H.L., 1967. Flood deposits, bijou creek, Colorado, june 1965. J. Sediment. Res. 37, 829–851. https://doi.org/10.1306/74D717B2-2B21-11D7-8648000102C1865D.
- Mumpy, A.J., Jol, H.M., Kean, W.F., et al., 2007. Architecture and sedimentology of an active braid bar in the Wisconsin River based on 3-D ground penetrating radar. In: Special Paper 432: Stratigraphic Analyses Using GPR. Geological Society of America, pp. 111–131. https://doi.org/10.1130/2007.2432(09.
- Murray, A.B., Paola, C., 2003. Modelling the effect of vegetation on channel pattern in bedload rivers. Earth Surf. Process. Landforms 28, 131–143. https://doi.org/ 10.1002/esp.428.
- Okazaki, H., Kwak, Y., Tamura, T., 2015. Depositional and erosional architectures of gravelly braid bar formed by a flood in the Abe River, central Japan, inferred from a three-dimensional ground-penetrating radar analysis. Sediment. Geol. 324, 32–46. https://doi.org/10.1016/j.sedgeo.2015.04.008.
- Paola, C., Borgman, L., 1991. Reconstructing random topography from preserved stratification. Sedimentology 38, 553–565. https://doi.org/10.1111/j.1365-3091.1991.tb01008.x.
- Puig, J.M., Cabello, P., Howell, J., et al., 2019. Three-dimensional characterisation of sedimentary heterogeneity and its impact on subsurface flow behaviour through the braided-to-meandering fluvial deposits of the Castissent Formation (late Ypresian, Tremp-Graus Basin, Spain). Mar. Petrol. Geol. 103, 661–680.

- https://doi.org/10.1016/j.marpetgeo.2019.02.014.
- Reinfelds, I., Nanson, G., 1993. Formation of braided river floodplains, Waimakariri River, New Zealand. Sedimentology 40, 1113—1127. https://doi.org/10.1111/j.1365-3091.1993.tb01382.x.
- Rice, S.P., Church, M., Wooldridge, C.L., et al., 2009. Morphology and evolution of bars in a wandering gravel-bed river; lower Fraser river, British Columbia, Canada. Sedimentology 56, 709–736. https://doi.org/10.1111/j.1365-3091.2008.00994.x.
- Rust, B.R., 1972. Structure and process in a braided river. Sedimentology 18, 221–245. https://doi.org/10.1111/j.1365-3091.1972.tb00013.x.
- Sambrook Smith, G.H., Ashworth, P.J., Best, J.L., et al., 2009. The sedimentology and alluvial architecture of a large braid bar, rio parana, Argentina. J. Sediment. Res. 79, 629–642. https://doi.org/10.2110/jsr.2009.066.
- Sambrook Smith, G.H., Ashworth, P.J., Best, J.L., et al., 2006. The sedimentology and alluvial architecture of the sandy braided South Saskatchewan River, Canada. Sedimentology 53, 413–434. https://doi.org/10.1111/j.1365-3091.2005.00769.x.
- Sambrook Smith, G.H., Ashworth, P.J., Best, J.L., et al., 2005. The morphology and facies of sandy braided rivers: some considerations of scale invariance. In: Blum, M.D., Marriott, S.B., Leclair, S.F. (Eds.), Fluvial Sedimentology VII. Wiley, Hoboken, pp. 145–158. https://doi.org/10.1002/9781444304350.ch9.
- Sambrook Smith, G.H., Best, J.L., Ashworth, P.J., et al., 2010. Can we distinguish flood frequency and magnitude in the sedimentological record of rivers? Geology 38, 579–582. https://doi.org/10.1130/G30861.1.
- Schumm, S.A., Khan, H.R., 1972. Experimental study of channel patterns. Geol. Soc. Am. Bull. 83, 1755. https://doi.org/10.1130/0016-7606(1972)83[1755:ESOCP]
- Schuurman, F., Kleinhans, M.G., 2015. Bar dynamics and bifurcation evolution in a modelled braided sand-bed river. Earth Surf. Process. Landforms 40, 1318–1333. https://doi.org/10.1002/esp.3722.
- Schuurman, F., Marra, W.A., Kleinhans, M.G., 2013. Physics-based modeling of large braided sand-bed rivers: bar pattern formation, dynamics, and sensitivity: braided river modeling. J. Geophys. Res. Earth Surf. 118, 2509–2527. https:// doi.org/10.1002/2013JF002896.
- Schuurman, F., Ta, W., Post, S., et al., 2018. Response of braiding channel morphodynamics to peak discharge changes in the Upper Yellow River. Earth Surf. Process. Landforms 43, 1648–1662. https://doi.org/10.1002/esp.4344.
- Skelly, R.L., Bristow, C.S., Ethridge, F.G., 2003. Architecture of channel-belt deposits in an aggrading shallow sandbed braided river: the lower Niobrara River, northeast Nebraska. Sediment. Geol. 158, 249–270. https://doi.org/10.1016/ S0037-0738(02)00313-5.
- Straub, K.M., Ganti, V., Paola, C., et al., 2012. Prevalence of exponential bed thickness distributions in the stratigraphic record: experiments and theory. J. Geophys. Res. 117, 2011JF002034. https://doi.org/10.1029/2011JF002034.
- Strick, R.J.P., Ashworth, P.J., Sambrook Smith, G.H., et al., 2019. Quantification of bedform dynamics and bedload sediment flux in sandy braided rivers from airborne and satellite imagery. Earth Surf. Process. Landforms 44, 953–972. https://doi.org/10.1002/esp.4558.
- Van De Lageweg, W.I., Van Dijk, W.M., Kleinhans, M.G., 2013. Morphological and stratigraphical signature of floods in a braided gravel-bed river revealed from flume experiments. J. Sediment. Res. 83, 1032–1045. https://doi.org/10.2110/jsr.2013.70.
- Vesipa, R., Camporeale, C., Ridolfi, L., 2017. Effect of sampling time in the laboratory investigation of braided rivers. Water Resour. Res. 53, 5184–5197. https:// doi.org/10.1002/2017WR020474.
- Warburton, J., Davies, T., 1994. Variability of bedload transport and channel morphology in a braided river hydraulic model. Earth Surf. Process. Landforms 19, 403–421. https://doi.org/10.1002/esp.3290190503.
- Williams, P.F., Rust, B.R., 1969. The sedimentology of a braided river. J. Sediment. Petrol. 39, 649–679.
- Wooldridge, C.L., Hickin, E.J., 2005. Radar architecture and evolution of channel bars in wandering gravel-bed rivers: fraser and squamish rivers, British Columbia, Canada. J. Sediment. Res. 75, 844—860. https://doi.org/10.2110/jsr.2005.066.
- Yao, Z.Q., Yu, X.H., Shan, X., et al., 2018. Braided-meandering system evolution in the rock record: implications for climate control on the Middle—Upper Jurassic in the southern Junggar Basin, north-west China. Geol. J. 53, 2710—2731. https:// doi.org/10.1002/gj.3105.
- Zang, D.S., Bao, Z.D., Li, M.Y., et al., 2020. Sandbody architecture analysis of braided river reservoirs and their significance for remaining oil distribution: a case study based on a new outcrop in the Songliao Basin, Northeast China. Energy Explor. Exploit. 38, 2231–2251. https://doi.org/10.1177/0144598720951280.
- Zhang, C.M., Yin, T.J., Wu, S.H., et al., 2022. Architectural Element analysis of non-marine oil and gas reservoir in China, the research history, progress and future trend: a review. Interpretation 1–103. https://doi.org/10.1190/int-2022-0030.1.
- Zhang, K., Wu, S.H., Feng, W.J., et al., 2020. Bar dynamics in a sandy braided river: insights from sediment numerical simulations. Sediment. Geol. 396, 105557. https://doi.org/10.1016/j.sedgeo.2019.105557.
- Zhang, X.G., Lin, C.Y., Zhang, T., 2010. Seismic sedimentology and its application in shallow sea area, gentle slope belt of Chengning uplift. J. Earth Sci. 21, 471–479. https://doi.org/10.1007/s12583-010-0108-y.